Volume 18 | Number 11 | 7 June 2018 | Pages 1507–1662

Lab on a Chip

Devices and applications at the micro- and nanoscale

rsc.li/loc

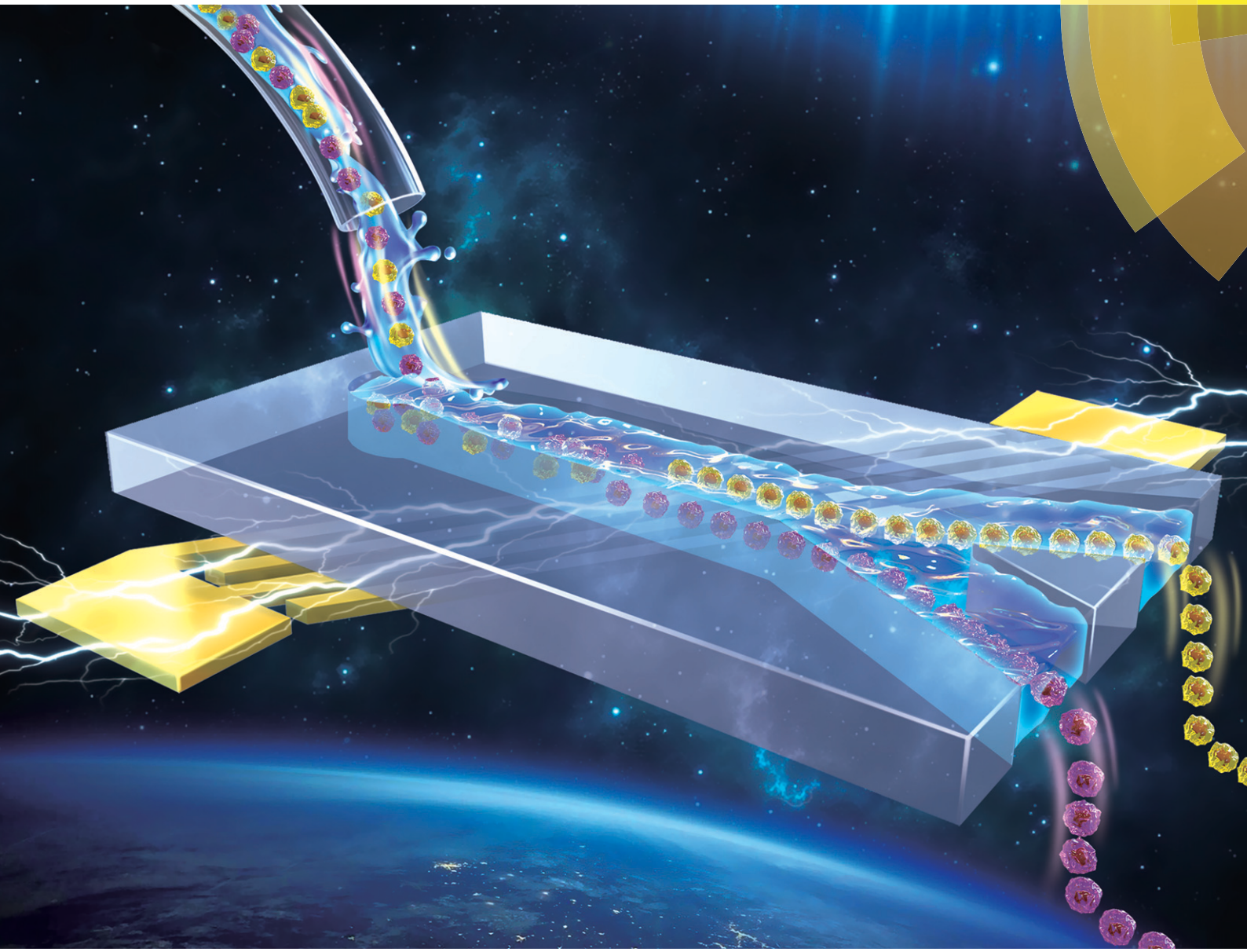

ISSN 1473-0197

ROYAL SOCIETY OF CHEMISTRY

PAPER

Dong Sun *et al.*

A simplified sheathless cell separation approach using combined gravitational-sedimentation-based prefocusing and dielectrophoretic separation

Lab on a Chip

PAPER

View Article Online
View Journal | View Issue

Cite this: *Lab Chip*, 2018, **18**, 1521

A simplified sheathless cell separation approach using combined gravitational-sedimentation-based prefocusing and dielectrophoretic separation†

Tao Luo,[a] Lei Fan,[a] Yixiao Zeng,[b] Ya Liu,[a] Shuxun Chen,[a] Qiulin Tan,[b] Raymond H. W. Lam[a] and Dong Sun*[a]

Prefocusing of the cell mixture is necessary for achieving a high-efficiency and continuous dielectrophoretic (DEP) cell separation. However, prefocusing through sheath flow requires a complex and tedious peripheral system for multi-channel fluid control, hindering the integration of DEP separation systems with other microfluidic functionalities for comprehensive clinical and biological tasks. This paper presented a simplified sheathless cell separation approach that combines gravitational-sedimentation-based sheathless prefocusing and DEP separation methods. Through gravitational sedimentation in a tubing, which was inserted into the inlet of a microfluidic chip with an adjustable steering angle, the cells were focused into a stream at the upstream region of a microchannel prior to separation. Then, a DEP force was applied at the downstream region of the microchannel for the active separation of the cells. Through this combined strategy, the peripheral system for the sheath flow was no longer required, and thus the integration of cell separation system with additional microfluidic functionalities was facilitated. The proposed sheathless scheme focused the mixture of cells with different sizes and dielectric properties into a stream in a wide range of flow rates without changing the design of the microfluidic chip. The DEP method is a label-free approach that can continuously separate cells on the basis of the sizes or dielectric properties of the cells and thus capable of greatly flexible cell separation. The efficiency of the proposed approach was experimentally assessed according to its performance in the separation of human acute monocytic leukemia THP-1 cells from yeast cells with respect to different sizes and THP-1 cells from human acute myelomonocytic leukemia OCI-AML3 cells with respect to different dielectric properties. The experimental results revealed that the separation efficiency of the method can surpass 90% and thus effective in separating cells on the basis of either size or dielectric property.

Received 12th February 2018,
Accepted 27th April 2018

DOI: 10.1039/c8lc00173a

rsc.li/loc

Introduction

The separation and purification of cells are the necessary pretreatment processes in disease diagnosis and therapy.[1] Various active and passive separation methods have been developed for separating heterogeneous cells in blood.[2] Active separation methods are generally based on magnetophoresis,[3–6] optics,[7,8] dielectrophoresis[9–11] and acoustophoresis,[12,13] which impose external forces to displace cells for separation. Passive separation methods include hydrophoretic[14,15] and hydrodynamic filtration,[16–18] pinched-flow fractionation,[19] inertial,[20–22] dean flow[23,24] and gravitational sedimentation,[25] which are based on the intrinsic physical properties (size, shape, density and elasticity) of cells. Passive separation methods are simple and have high throughput, whereas active methods provide greater control flexibility. In contrast to magnetophoresis[26] and optics,[27] which require additional 'tags' or 'labels' for cell identification, dielectrophoretic (DEP) separation is a label-free process, thereby simplifying sample preprocessing. It also separate cells without specific biomarkers by considering the differences in size and dielectric property.

Over the past decades, various strategies, such as DEP-field flow fractionation (DEP-FFF) and 3D lateral DEP (LDEP), have been used for the precise separation of biological cells on the basis of size difference.[11,28–33] In recent years, the DEP method has been applied for the separation of cells with

[a] *Department of Mechanical and Biomedical Engineering, City University of Hong Kong, Hong Kong, China. E-mail: medsun@cityu.edu.hk; Tel: (+852) 3442 8405*
[b] *Key Laboratory of Instrumentation Science and Dynamic Measurement, Ministry of Education, North University of China, Taiyuan, China*

† Electronic supplementary information (ESI) available. See DOI: 10.1039/c8lc00173a

similar sizes, such as human mesenchymal stem cells and their differentiation progenies (osteoblasts), on the basis of the difference in dielectric property.[34] However, most of the reported DEP separators require sheath flow or well-designed electrodes for the active prefocusing of an inputted cell mixture to the side/centre of a microfluidic channel before it enters the DEP separation region. The use of sheath flow requires a complex and cumbersome peripheral system for multi-channel fluid control, and this requirement hinders the integration of DEP separation systems with other microfluidic functionalities. Moreover, the use of a sheath buffer dilutes the samples and reduces the actual throughput of the sample processing.[35] Majority of existing electric prefocusing methods employ dielectrophoresis or electro-osmosis. Dielectrophoresis highly depends on the DEP forces of particles and requires well-designed electrode structures. As such, a cell mixture with large differences in size and dielectric property is difficult to focus.[36] Although electro-osmosis can focus cells with different sizes and dielectric properties into a stream, the focusing efficiency is low when the flow rate is high (>1 μL min^{-1}), and thus its application in high-throughput sample processing remains limited.[37–39] In this regard, passive sheathless cell prefocusing can be combined with active DEP separation for the simple, label-free, and high-throughput separation of cells on the basis of size and dielectric property.

Four methods are generally used for the passive sheathless focusing of cells. The first method is microfluidic inertial focusing, which uses the inertial lift and drag forces induced by secondary flows to confine the focusing position.[40] By using this method, cells with a high throughput can be precisely focused through specific a design in the microchannel.[41–43] The second method is hydrophoretic cell focusing. Relying on the transverse flows generated by the anisotropic fluidic resistance along the width of the channel, this method can focus cells to the side or centre of a channel.[44] The third method is deterministic lateral displacement (DLD), which navigates cells through an array of posts for sheathless cell focusing.[45,46] The fourth method is viscoelastic focusing. This method is based on the migration of cells in viscoelastic fluids, which is usually dominated by both inertial and viscoelastic effect.[47–50] All these four methods can be used for separating cells with different sizes, but none of them can easily separate cells with a uniform size distribution.

In a number of approaches, passive and active methods have been combined for separating cells with higher efficiency. For instance, multi-orifice flow fractionation was combined with dielectrophoresis for the separation of breast cancer cells from blood samples in a label-free and continuous manner.[21] However, this method was still based on the size difference between the cancer and blood cells. Hydrophoretic method have been combined with DEP method for size-based cell separation[51] and plasma isolation[52] from diluted whole blood. This combination enabled to control the lateral positions of particles by modulating the external voltages without redesigning the microfluidic channel, which demonstrated great flexibility.[53] However, the separation of cells based on this combination was still size-dependent, and the prefocusing efficiency was highly dependent on the DEP response of the cell samples. By combining DLD with DEP technology, tunable and high resolution separation of cells with respect to both size and polarizability can be achieved.[54] The design and fabrication accuracy of the DLD chips were highly dependent on the size distribution of the cell samples. Several approaches combined inertial cell focusing and the downstream magnetic field for the separation of magnetically labelled circulating tumour cells (CTCs) from leukocytes[26] and separate magnetically labelled leukocytes from CTCs.[55] However, this method was not label-free and therefore unsuitable for the separation of previously unknown cell subpopulations. Overall, the design of the microfluidic channel for inertial, hydrophoretic and DLD chips highly depend on the size of cells to be handled, and this dependence limits the flexibility of these methods for different samples.

In this paper, we proposed a novel approach that combines gravitational-sedimentation-based sheathless prefocusing and DEP separation in a simple microfluidic setup for the continuous separation of cells on the basis of either size or dielectric property. This approach exhibited two unique advantages. Firstly, from the perspective of sheathless focusing, this method utilised the gravitational sedimentation of cells in a tubing for the sheathless focusing of a cell mixture in a wide range of flow rates. In this method, cell focusing mode can be adjusted to the upper or lower side or the centre of the microfluidic channel by changing the tubing steer angle. This method can focus a cell mixture with diverse size distributions or dielectric properties into the same stream in a microfluidic channel, by simply adjusting the tubing length and the diameter. Given that modifications in the designs of microfluidic channels are unnecessary for the processing of different cell samples, this method offered greater flexibility than that of other passive focusing methods, such as inertial and hydrophoretic methods. Secondly, from the perspective of cell separation, this method utilised an oblique interdigitated electrode array located at the bottom of the microchannel for the generation of a non-uniform electric field and production of a positive DEP force for cell manipulation. Under the resultant DEP force and hydrodynamic drag force (F_H), the cells with different sizes or dielectric properties move along different trajectories and became separated. The effectiveness of the approach in separating cells according to size variation was verified through experiments on a mixture of yeast cells (diameter: approximately 6 μm) and THP-1 cells (diameter: approximately 13 μm). Then, the effectiveness of the approach in separating cells with uniform sizes but different dielectric properties was verified through experiments on a mixture of OCI AML3 (diameter: approximately 13 μm) and THP-1 (diameter: approximately 13 μm) cells. The experimental results indicated that the separation efficiency can exceed 90%, implying that the proposed approach can effectively separate

cells on the basis of variations either in their sizes or in their dielectric properties.

Materials and methods

Design and fabrication of the DEP separator

The designed chip consisted of platinum (Pt) electrodes and a polydimethylsiloxane (PDMS) microchannel with one inlet and two outlets, as shown in Fig. 1A. The entire chip can be separated into three functional regions, namely, sheathless cell focusing region, label-free DEP separation region and outlets. The sheathless cell focusing region consisted of a tubing inserted into the inlet. The tubing had a proper steering angle θ with the direction of the flow (x-direction in Fig. 1A). When flowing forward in the tubing, the widely-dispersed cells would gradually sediment to the bottom wall of tubing due to gravitation. This sedimentation makes cells focused in Z direction, and the Z-axis focused cells are fed into the inlet of the downstream separation channel. By this way, the cells are focused along X direction in the separation channel before they flow into the DEP separation region, which is normally implemented by sheath flow for achieving high-efficient downstream cell separation. The DEP separation region had a microfluidic channel that was 1 mm wide and 14 mm long (Fig. S1†). The microelectrodes were composed of 40 interdigitated pairs and aligned to the microchannel at an angle of 45° (Fig. S1† and 1B). Both the width and gap of the platinum (Pt) electrodes were 50 μm. Two outlets with widths of 634 and 891 μm were used for the collection of the separated cells (Fig. S1† and 1B). Before flowing into the DEP separation region, all the cells were focused to the upper side of the channel. When passing through the DEP separation region, cells subjected to a stronger DEP force flowed into outlet 2, whereas cells subjected to a weaker DEP force flowed into outlet 1. The DEP force F_{DEP} can be given as $F_{DEP} = 2\pi\varepsilon_m r^3 \mathrm{Re}[K(\omega)]\nabla E^2$, where ε_m is the absolute permittivity of the suspending medium, r is the radius of the cell, ∇E^2 is the gradient of the square of the applied electric field E, and $K(\omega)$ refers to the Clausius–Mossotti (CM) factor.[53] Re means the real part of the CM factor, $K(\omega)$ depends on the complex permittivity of the cell and the suspending medium, and the frequency of the external electric field. $K(\omega)$ can be given as $K(\omega) = (\varepsilon^*_{cell} - \varepsilon^*_{medium})/(\varepsilon^*_{cell} + 2\varepsilon^*_{medium})$, where $\varepsilon^* = \varepsilon - i\sigma/\omega(i^2 = -1)$ is the complex permittivity, σ is the electrical conductivity, and ω is the frequency of the electric field. It is obvious to see that DEP force is a function of particle size and dielectric parameters, and cells of different sizes or different dielectric properties experience different DEP forces, which enables them to be successfully separated (Fig. 1A).

The fabrication processes of the DEP separator were mainly based on soft-lithography and lift-off technologies. As shown in Fig. S2,† oblique interdigitated microelectrode arrays were patterned on a glass substrate (25 mm × 50 mm) by using lift-off technology through the following procedures. Firstly, a 2 μm-thick positive photoresist (PR) RZJ304 film was spin-coated on a cleaned glass. After baking at 100 °C for 2 min, the substrate was exposed to 365 nm UV light at an intensity of 12 mJ cm^{-2} for 5 s and then developed using a RZX-3038 developer for 30 s to define the PR pattern. Then, a 200 nm-thick Pt film was deposited onto the PR-patterned glass, and the PR was subsequently removed with the PR stripper for 5 min. Fig. S2† illustrates the fabrication processes for the PDMS microchannel. A silicon wafer of 4 inches in diameter was used as the substrate and spin-coated with a 30 μm thick layer of negative PR SU-8 2050 (Microchem Corp.). After prebaking, exposure, postbaking and development, the SU-8 mould for PDMS microchannel production was obtained. Appropriate amounts of PDMS (Sylgard 184, Dow Corning) and curing agent were mixed at a ratio of 10 : 1 by weight and poured in the fabricated SU-8 mould. The mould with the PDMS mixture was placed in a vacuum oven for the removal of air bubbles and curing of the PDMS by baking at 70 °C for 2 h. Finally, the cured PDMS microchannel was peeled off from the mould, then punched at the inlet and outlets, and finally bonded with the Pt electrodes *via* oxygen plasma treatment (Fig. S2†). As shown in Fig. 1C, copper wires were soldered on the microelectrode pads of the fabricated microfluidic chip. The inlet and outlets of the chip were connected to polyethylene (PE) tubes for sample injection and collection. Both sides of the electrodes were connected to a signal generator with the use of copper wires to generate a non-uniform electric field in the microchannel for deflecting cells.

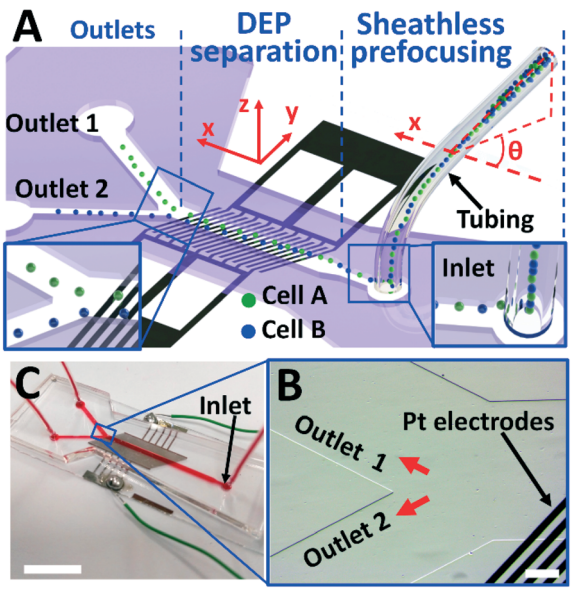

Fig. 1 Design of the microfluidic cell separator. (A) Schematic of the cell separator containing an inlet and two outlets. (B) Photograph of the cell separator with red ink in the microfluidic channel for visualization. Scale bar = 2 cm. (C) Bright-field microscopic image of the cell separation region. Scale bar = 200 μm.

Finite element analysis

Simulations were performed by using 3D CFD models on COMSOL Multiphysics for the prediction of cell trajectories in the tubing and their variations when the flow rates and

diameters of the tubing and cells were modified. For the simplification of the model and reduction of solution time, the study was conducted in two aspects. In the first aspect, a stationary CFD problem was solved by using the physics of laminar flow, where the cells were excluded. Multiblock structured meshes with approximately six million cells and near-wall refinement were used. In this way, a standard Hagen–Poiseuille flow solution can be obtained for the tubing with a circular cross-section. In the second aspect, the time-dependent cell trajectories were solved by using the physics of particle tracing for fluid flow. A total of 100 cells uniformly dispersed at the inlet were released at 0 s. Drag force and gravity were applied to calculate the cell trajectories. Different flow rates were implemented at the inlet, and a zero-pressure boundary condition was set at the outlet. No slip boundary condition was applied at the channel walls. The flow rates and diameter of the cells and the tubing were parameterised to investigate the effects of flow and geometry parameters on the cell trajectories. The physical properties of water were considered in fluid, and the density of particle ρ_p was set to 1070 kg m^{-3} in accordance with a previous work.[56] The required minimum tubing length L_{min} and diameter D (Fig. 2A) for the complete sedimentation of cells in the tubing can be obtained based on the simulated cell trajectories. 3D CFD models were also used for the prediction of the flow patterns (trajectories) of the cells in the microfluidic channel. Here, only the physics of the laminar flow was used for solution of the stationary CFD problem. The cell trajectories in the microchannel were visualised with respect to different steering angles of the tubing through the use of streamlines.

Cell and device preparation

The OCI-AML3 cells were cultured in 80% alpha-MEM (Sigma, St Louis, MO) supplemented with 20% h.i. FBS (Atlanta Biologicals, GA). THP-1 cells were cultured in RPMI 1640 medium (Sigma, St Louis, MO) supplemented with 10% fetal bovine serum (Atlanta Biologicals, GA). All of the cells were incubated at 37 °C under a 5% CO_2 atmosphere prior to the experiments. Immediately prior to the DEP experiments, the OCI-AML3 and THP-1 cells were firstly stained with fluorescent dye, *i.e.*, CFDA-SE for green fluorescence and Hoechst 33342 for blue fluorescence. Then, the cells were washed twice with 1 mL PBS and suspended in an isotonic low-conductivity DEP buffer, which contained 8.6% w/w sucrose, 0.3% w/w dextrose and sufficient PBS to increase the conductivity of the solution

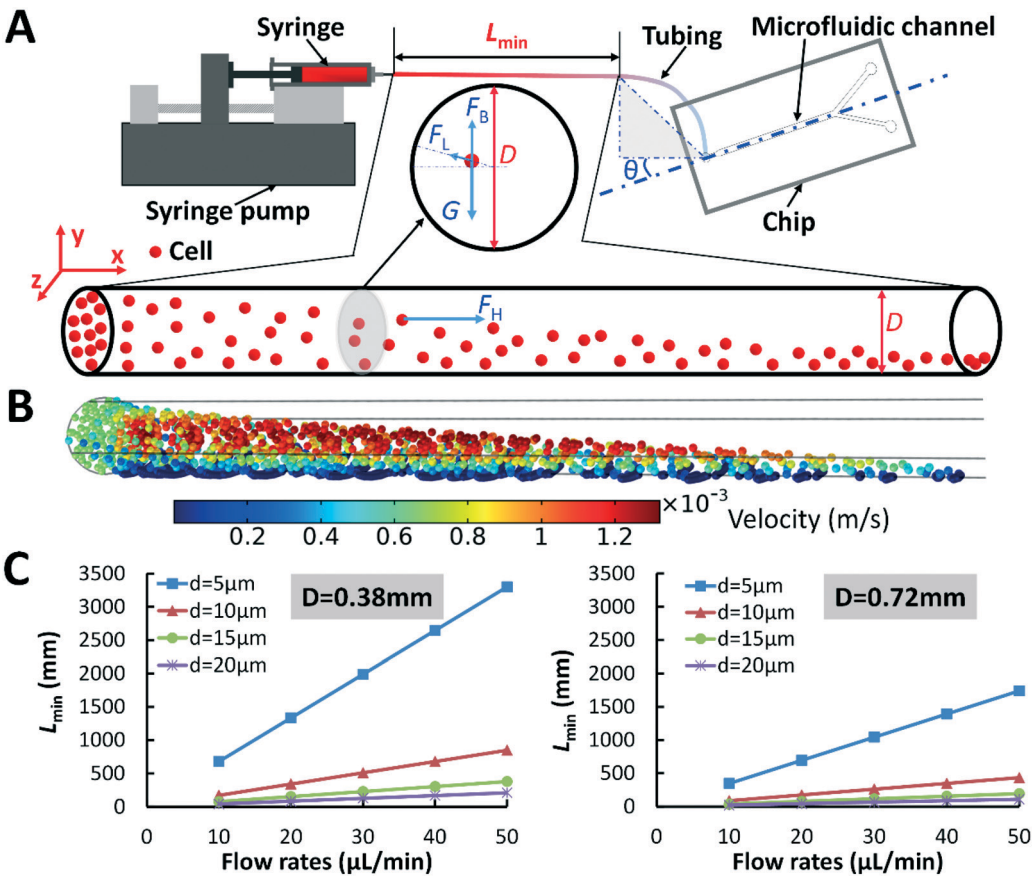

Fig. 2 Operation principle of using gravitational sedimentation for sheathless cell focusing. (A) Schematic of experimental setup for using gravitational sedimentation of cells in a tubing to achieve sheathless cell focusing in the microfluidic channel. (B) Simulated cell trajectory pattern in the tubing by using COMSOL Multiphysics software. (C) Minimum tubing length L_{min} for complete sedimentation of cells in the tubing *versus* the input flow rate under different *d* (diameter of the cell) and *D* (inner diameter of the tubing).

to 400 μS cm^{-1} at pH 7.4. Prior to each experiment, the microfluidic chips were cleaned using ethanol and deionised water for sterilisation and bubble removal, and treated with 1% BSA (Sigma, St Louis, MO) to precoat the microchannel to prevent the nonspecific adhesion of cells.

Experimental procedures

The cell suspension was injected into the inlet of the microchannel through the tubing connected to a syringe pump (LSP01-2A, Longer Pump) with a 1 mL syringe. Sinusoidal voltage was applied between the microelectrodes by using a function signal generator (AFG-3081, GWIUSTEK), which was connected to the electrode pads of the DEP chip. The steering angle of the tubing was firstly fixed at 30° to achieve reliable cell focusing along the upper side of the microfluidic channel at the downstream region. Subsequently, the frequency and magnitude of the applied voltage were adjusted to achieve efficient cell separation. The cell trajectories were observed and recorded using a microscope (Axio Vert. A1, Zeiss) with a CCD camera (Axiocam 105 colour, Zeiss). The numbers of cells collected from the inlet and outlets were counted using a haemocytometer (Marienfeld, Germany) for quantitative analysis.

Cell viability test

The cells collected from the inlet and outlets were washed twice by adding 1 mL of PBS. Then, 1 mL of diluted propidium iodide (PI) was added to the staining buffer (50 μg mL^{-1}). Finally, the cells were incubated for 5 min at 37 °C and analysed by microscopy images to count the viability of cells. Only dead cells showed red fluorescence. Cell viability was defined as the ratio of the number of cells without showing red fluorescence over the total number of cells.

Data analysis

All recorded images were analysed and processed using ImageJ (http://rsb.info.nih.gov/ij/). The efficiency of separation was defined as the ratio of the number of a type of cells collected at the expected outlet over the total number of the same type of cells collected at all outlets. Purity was defined as the ratio of the number of a type of cells collected at an outlet over the total number of all cells collected at the same outlet. All experiments were repeated for at least three times.

Results and discussions

Gravitational sedimentation of non-neutrally buoyant cells in tubing

Biological cells are generally considered neutrally buoyant when suspended in culture media or PBS buffer. However, in reality, many cells have densities that are slightly greater than that of blood plasma, culture media, and PBS buffer[57–60] (Table S1†), implying that most cells present gravitational sedimentation when suspended in liquids such as culture media and PBS buffer. As shown in Fig. 2A, the suspended cells were pumped into the microfluidic chip through a capillary tubing. The cell trajectories in the tubing were affected by buoyant force F_B, gravity G, net inertial lift force F_L, and hydrodynamic drag force F_H. F_B, G and F_L affected the lateral motion of the cells, whereas F_H triggered the cells to move forward along the axial direction of the tubing (Fig. 2A). The F_L at a very low Reynolds number (Re) can be disregarded (Fig. S3†).[40] In this work, a low Re close to zero was calculated according to $Re = \rho_f UD/\mu$, where ρ_f is the fluid density. The fluid used in the experiments of this study is DEP buffer, which has the density of 1016 kg m^{-3} (Table S1†). U is the average velocity, μ is the dynamic viscosity and D is the characteristic channel dimension, *i.e.* the diameter of the circular cross-section of the tubing. Thus, the lateral motion of the cells was dominated by the net force of gravity and buoyant force. The net force was defined as $G - F_B = (\rho_c - \rho_f) \times V_c \times g$, where ρ_c is the cell density. THP-1, OCI-AML3 and yeast cells used in this study have the densities of 1070, 1070 and 1100 kg m^{-3}, respectively (Table S1†). V_c is the volume of a single cell and $g = 9.8$ m s^{-2} is the acceleration of gravity.

Cells gradually sedimented when flowing through the tubing, and all of the cells can sediment to the bottom of the tubing if the tubing was sufficiently long. The minimum tubing length L_{min} that allowed all of the cells to sediment to the bottom of the tubing was obtained through CFD simulation (Fig. 2B and Video S1†). In addition, the relationship between L_{min} and other parameters, such as the flow rates and diameters of the cells and the tubing was quantitatively characterised based on the simulation results (Fig. 2C). L_{min} linearly increased with as the input flow rates increased. The cells with smaller sizes required a tubing with a longer length for sedimentation, and increasing the diameter of the tubing reduced L_{min}. On the basis of the flow rate requirement for the DEP cell separation (for which the flow rates cannot exceed 30 μL min^{-1}; otherwise, the DEP force would not be sufficiently large to deflect the cells), the tubing availability (tubing diameter: 0.38 mm) and the size distribution of the cells used in this study (Fig. S4†), the tubing length of 400 mm was selected for subsequent experiments in this study.

To visualise the cell sedimentation in the tubing, a microfluidic chip with an inlet located at the centre of a circular channel and a 360° opened outlet was designed and fabricated (Fig. 3A and S5†). For the circular microfluidic channel, the cells flowed in a sector pattern when the cells sedimented to the bottom of the tubing, and the direction of the sector can be changed by adjusting the steer angle of the tubing. The flow patterns of the cells in the microfluidic channel under different flow rates and tubing steer angles are shown in Fig. 3. The THP-1 cells stained with green fluorescent dye CFDA-SE and suspended in DEP buffer were used for the experiments in this study. Fig. 3B illustrates that the cells flowed in a sector pattern in the microfluidic channel, as predicted by the simulated streamlines shown in Fig. 3A. The sector angle increased as the flow rates increased (Fig. 3B). As flow rate increased from 10 μL min^{-1} to 50 μL min^{-1}, most cells sedimented to the bottom of the tubing, and the sector angle increased slightly, indicating that the proposed cell

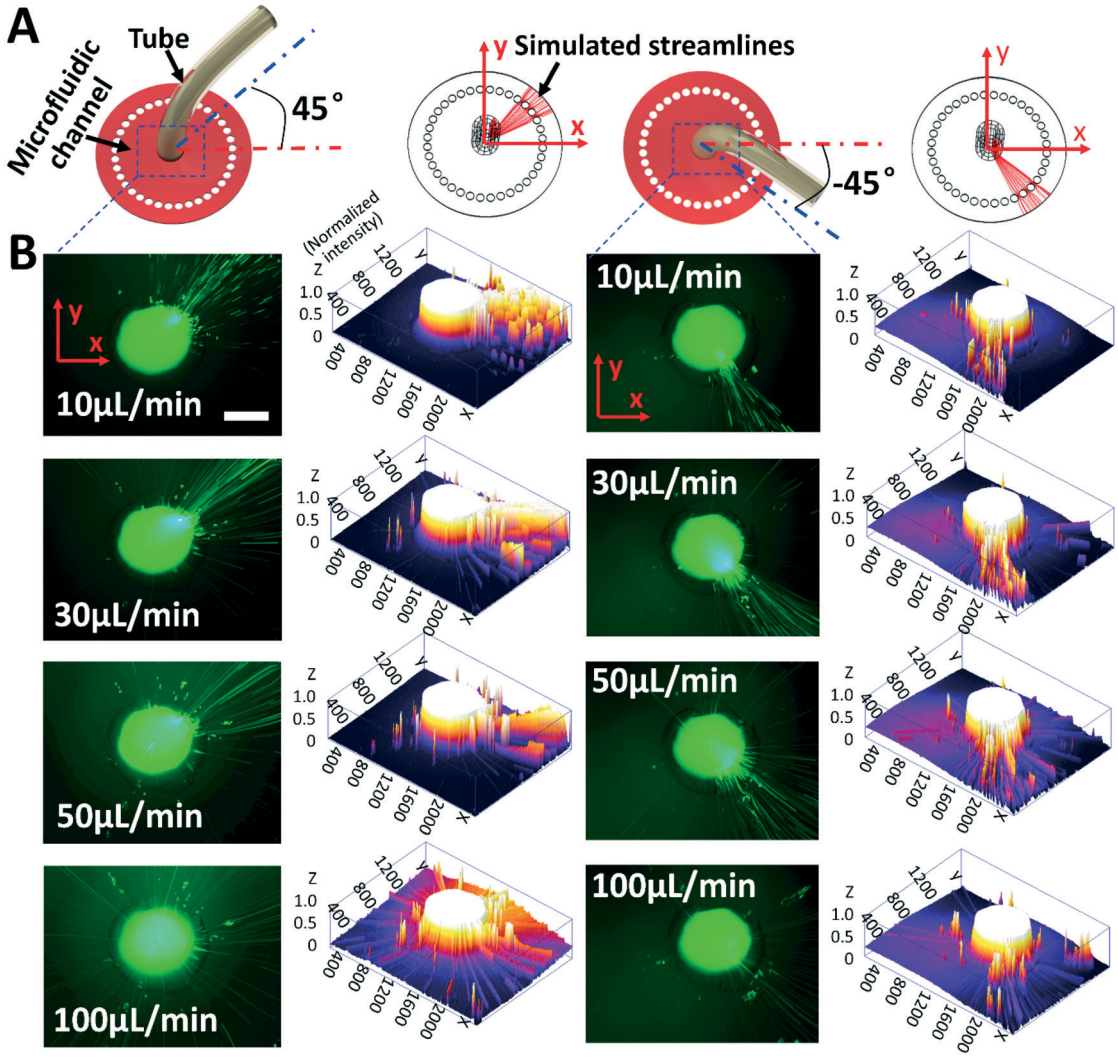

Fig. 3 Experimental study of gravitational sedimentation of cells in the tubing (Video S2†). (A) Schematic of experimental setup for studying gravitational sedimentation of cells in the tubing based on a designed microfluidic chip with an inlet and a 360°-opened outlet. (B) Results for cell flow pattern under different flow rates. THP-1 cells stained with green fluorescent dye CFDA-SE was suspended into DEP buffer. Cell flow pattern was characterised by the normalised fluorescence intensity. The diameter and length of the tubing are 0.38 and 400 mm, respectively. Scale bar = 300 μm.

focusing method was effective within a wide range of flow rates. When the flow rate was increased to 100 μL min^{-1}, a tubing of 400 mm was insufficiently long for most cells to be sedimented. Thus, the sector angle of the cell flow patterns was increased to 360°. Considering these experimental results, we anticipated that gravitational-sedimentation-based sheathless cell focusing can work within a wide range of flow rates by adjusting the tubing geometries. Moreover, changing the tubing angle can change the direction of the cell flow sector accordingly, indicating the potential of using gravitational sedimentation in the tubing for tuneable sheathless cell focusing in microfluidic channels for various applications.

Tubing steering angle regulated sheathless cell focusing in microfluidic channel

Fig. 4 illustrates the different cell flow patterns at a flow rate of 10 μL min^{-1} under six different tubing steer angles of the microfluidic channel in the proposed DEP separator. The THP-1 cells stained with green fluorescent dye CFDA-SE and suspended in DEP buffer were also used for this analysis. Schematics of different tubing steer angles were shown in Fig. 4A, and Fig. 4B illustrates the cell trajectories predicted by CFD simulation and visualised with red colour streamlines. Fig. 4C and D illustrate that six different cell flow patterns appeared for the different tubing steer angles. The cells were focused to flow along the lower side of the channel when the tubing steer angle was −30° and along the upper side of the channel when the tubing steer angle was 30°. In addition, the cells were focused to the centre of the channel and the position between the centre and upper side of the channel when the tubing steer angles were 180° and 120°, respectively. When the tubing steer angle was 0°, most of the cells flowed along either the upper or lower side of the channel, and a few cells became randomly distributed between the upper and lower side of the channel. When the tubing

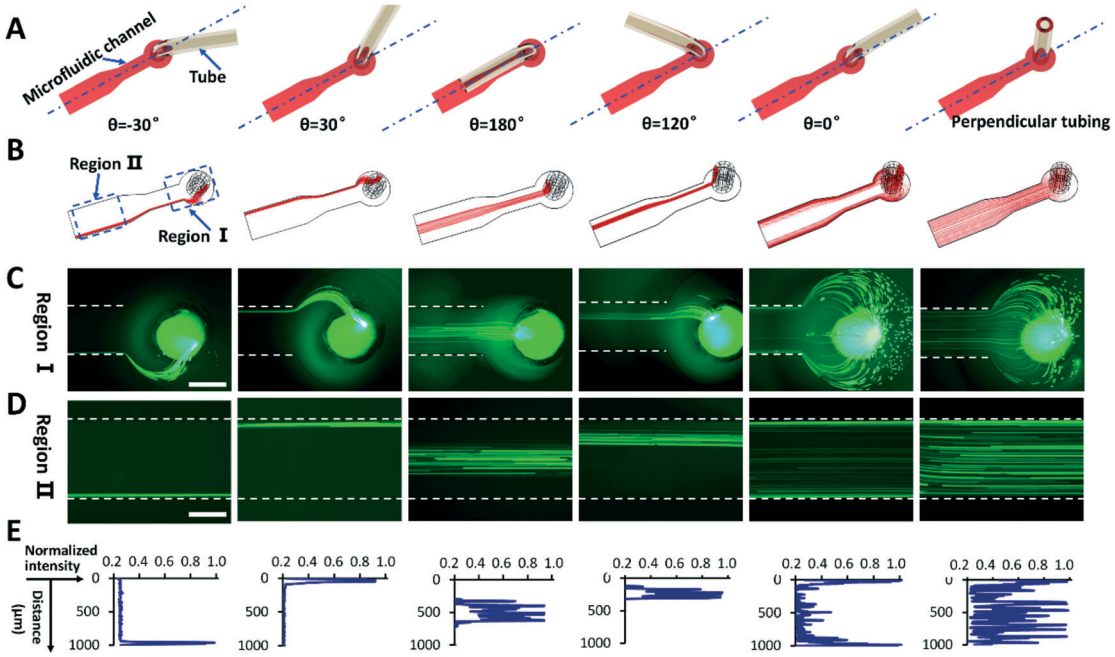

Fig. 4 Experimental study of using gravitational sedimentation of cells in the tubing for sheathless cell focusing in the microfluidic channel of the cell separator at the flow rate of 10 μL min^{-1} (Video S3†). (A) Schematic of changing steering angle of the tubing for achieving different cell flow patterns in the microfluidic channel. (B) Predicted cell flow patterns for different steering angles of the tubing by using CFD simulation (cell flow patterns was visualised with red streamlines). (C) Cell flow pattern results at region I of the microfluidic channel under different steering angles. THP-1 cells stained with green fluorescent dye CFDA-SE was suspended into DEP buffer. The diameter and length of the tubing are 0.38 and 400 mm, respectively. (D) Cell flow pattern results at region II of the microfluidic channel under different steering angles. (E) Illustration of cell distribution across the 1 mm wide channel at region II by using normalised fluorescence intensity. Scale bar = 500 μm.

was inserted into the inlet in the same direction as gravity, the cells did not sediment to one side of the channel and were uniformly distributed throughout the width of the microchannel. The cell distribution across the 1 mm wide channel at the region II (Fig. 4B) was quantitatively characterised with normalised fluorescence intensity (Fig. 4E).

The results in Fig. 4 demonstrated that the proposed gravitational sedimentation method can successfully achieve sheathless cell focusing. Different cell focusing modes can be selected by simply adjusting the steer angle of the tubing. Similarly, cells with different sizes can be focused into the same stream if the L_{min} for the smallest cells is used. In some applications, the cells may need to flow or be distributed uniformly in the channel at relatively low flow rates. In cases when the tubing length cannot be shortened, a tubing with a small diameter may be used, or the flow direction of the cells may be the same as that of gravity. Abrupt geometric alteration of the fluidic path may affect the cell focusing pattern in the microfluidic channel especially when vortex is generated in the connector. In this study, the PE tubing, which has a circular inner cross-section with uniform diameter, was directly inserted into the inlet of the chip. Thus, abrupt geometric alteration of the fluidic path of the connector was avoided. In addition, bending angle of the tubing with regard to the *X*–*Y* plane will not affect the gravitational sedimentation of cells in *Z* direction if the flow path in the tubing is long enough to make cells sediment completely, hence the change of bending angle of the tubing will have very slight influence on the cell focusing pattern in the microfluidic channel. Overall, in contrast to many existing approaches, such as sheath and inertial focusing methods, the proposed gravitational-sedimentation-based sheathless cell focusing offers unique advantages in simplicity and flexibility.

Size based separation of THP-1 cells from yeast cells

A case study of separating THP-1 cells from yeast cells was performed to demonstrate the effectiveness of the proposed approach for size-based cell separation. The average diameter of the yeast and THP-1 cells were approximately 6 and 13 μm, respectively (Fig. S4†). The mixed cell suspension was injected through a 400 mm long PE tubing with a steering angle of 30° (Fig. 4A) into the cell separator at a flow rate of 12.5 μL min^{-1}. In this situation, all of the cells were focused to the upper side of the channel and flowed into outlet 1 (Fig. 5A). When 5 MHz and 12 V_{p-p} sinusoidal voltage was applied, the cells deflected because of the net force of the hydrodynamic drag force and the DEP force. The values of CM factor of THP-1 and yeast cells were calculated based on data from literatures[61–63] (Table S2†). It is obvious that $\mathrm{Re}[K(\omega)] > 0$ at the working frequency of 5 MHz, which means that all the cells experienced positive DEP forces (Fig. S6†). The THP-1 cells deflected more obviously than the yeast cells because of their larger size. Therefore, most THP-1 cells flowed into outlet 2, whereas most yeast cells flowed into outlet 1. In this way, the two types of cells were successfully separated on the

proposed cell separator on the basis of size difference (Fig. 5B and Video S4†).

As shown in Fig. 5C, most of the yeast cells were collected at outlet 1, whereas most of the THP-1 cells were collected at outlet 2. The collection efficiency of the yeast cells at outlet 1 was 92.7%, and that of the THP-1 cells at outlet 2 was 92.8% (Fig. 5D). The purity of the yeast cells at outlet 1 was 88.1%, and that of the THP-1 cells at outlet 2 was 95.3% (Fig. 5E). These results verified the good separation performance of the proposed approach.

Dielectric property based separation of THP-1 cells from OCI-AML3 cells

We performed the second case study of separating of THP-1 cells from OCI-AML3 cells to demonstrate the effectiveness of the proposed dielectric-property-based separation approach. The THP-1 and OCI-AML3 cells were both acute myeloid leukemia (AML) cells with similar sizes (Fig. S4†). They are of different subtypes according to their maturity and the cell type that the leukaemia develops. According to the French–

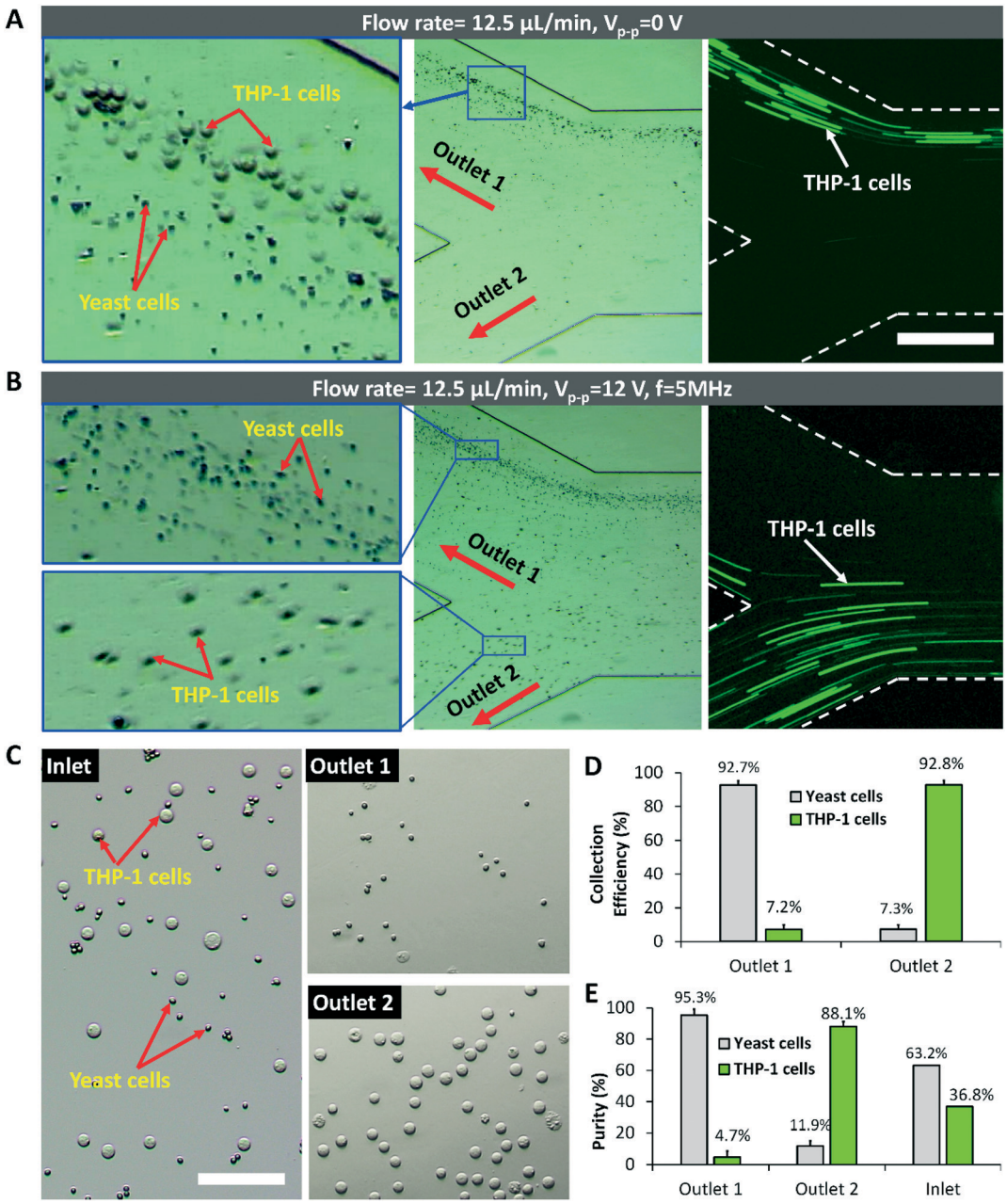

Fig. 5 Experimental results of size based separation of THP-1 cells (around 13 μm) from yeast cells (around 6 μm). (A) All cells were focused to the upper side of the channel and flowed into the outlet 1 at the flow rate of 12.5 μL min^{-1} when electric field is off. THP-1 cells were stained with green fluorescent dye CFDA-SE. Scale bar = 500 μm. (B) Yeast cells flowed into the outlet 1 and THP-1 cells flowed into outlet 2 when 5 MHz and 12 V_{p-p} sinusoidal signal was applied to the separator. (C) Microscopic images of cells collected from the inlet and two outlets. Scale bar = 100 μm. (D) Cell collection efficiency of two outlets. (E) Purity of cells in two outlets.

American–British (FAB) classification, the OCI-AML3 cells belonged to the FAB subtype M4, and the THP-1 cells belonged to the FAB subtype M5. These two types of cells can only be separated based on their different dielectric properties because the DEP force is related to both cell diameter and dielectric property (membrane capacitance, cytoplasm conductivity, *etc.*), and different dielectric properties result from the heterogeneity in cellular structures.[64] The mixed cell suspension was injected through a 400 mm long PE tubing with a steering angle of 30° (Fig. 4A) into the cell separator at a flow rate of 12.5 μL min^{-1}. The cells were focused to the upper side of the microfluidic channel before entering the DEP separation region (Fig. 4C and D). All the cells flowed into outlet 1 when the applied peak-to-peak voltage V_{p-p} was zero (Fig. 6A). When a 5 MHz and 12 V_{p-p} sinusoidal voltage was applied, the cells deflected because of the net force of the hydrodynamic drag force and the DEP force. As shown in Fig. S6,† $Re[K(\omega)] > 0$ at the working frequency of 5 MHz, which means that both THP-1 and OCI-AML3 cells experienced positive DEP forces. Most THP-1 cells deflected more obviously than the OCI-AML3 cells and flowed into outlet 2, whereas most OCI-AML3 cells flowed into outlet 1. In this way, the two types of cell subtypes were separated successfully by using the proposed cell separator (Fig. 6A and Video S5†).

Fig. 6B shows that most of the OCI-AML3 cells were collected at outlet 1, and most of the THP-1 cells were collected at outlet 2. The collection efficiency for OCI-AML3 at outlet 1 was 96.6%, and that of the for the THP-1 cells at outlet 2 was 91.4% (Fig. 6C). The purity of OCI-AML3 cells at outlet 1 was 91%, and that of THP-1 cells at outlet 2 was 97.3% (Fig. 6D). The sizes of these two cell subtypes were very similar, suggesting that they suffered from the similar hydrodynamic drag force. Therefore, the THP-1 cells must experience a considerably larger DEP force to separate from the OCI-AML3 cells.

Note that both the gravitational-sedimentation-based prefocusing and dielectrophoretic separation methods suffer from the limitation of low flow rate. Some approaches that can overcome this limitation have been reported in the literature. From the perspective of gravitational-sedimentation-based prefocusing, flow rate can be increased by using longer tubing or tubing with larger diameter, which has been demonstrated in the simulation as shown in Fig. 2. From the perspective of dielectrophoretic separation, flow rate can also be increased by increasing the DEP force or extending the flow

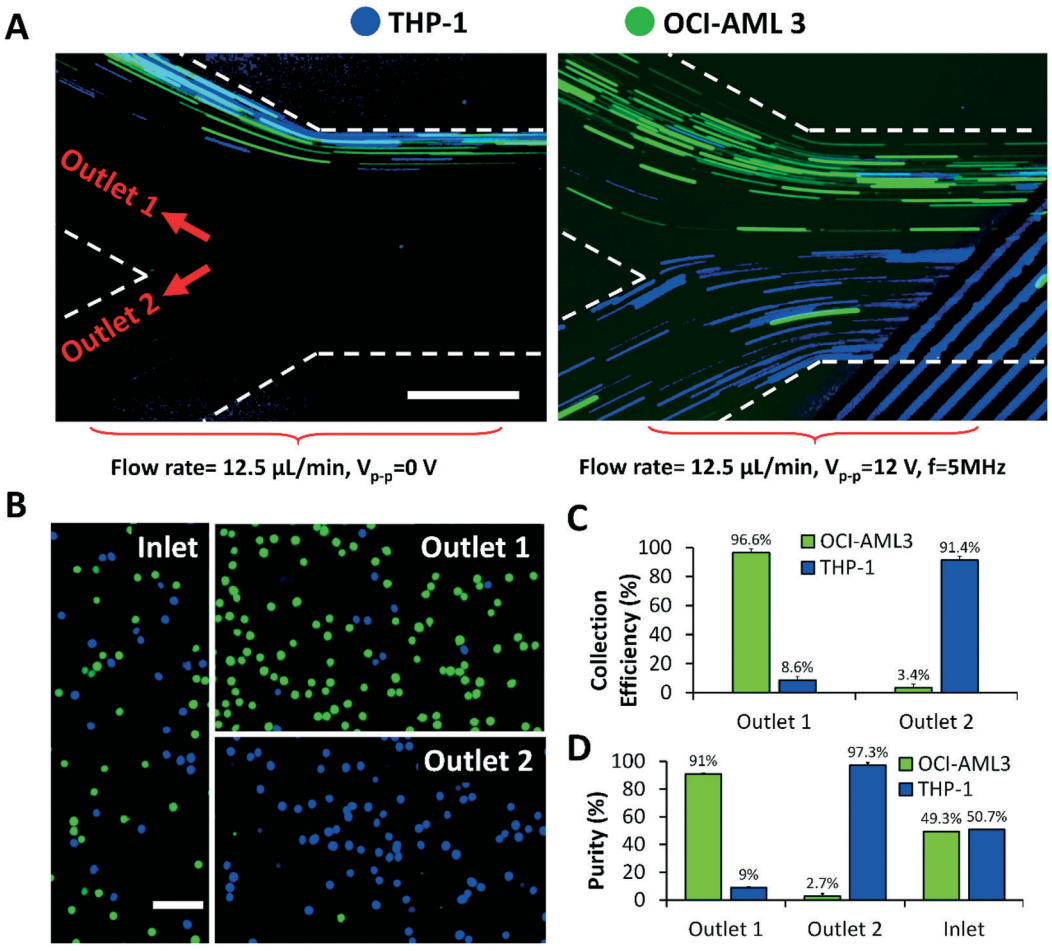

Fig. 6 Experimental results of dielectric property based separation of leukemic cell subpopulations (THP-1 and OCI-AML3 cells). (A) Composite fluorescence images showing the trajectories of THP-1 (blue) and OCI-AML3 (green) cells. Scale bar = 500 μm. (B) Composite fluorescence images of particles collected at the inlet and two outlets. Scale bar = 100 μm. (C) Cell collection efficiency of two outlets. (D) Purity of cells in two outlets.

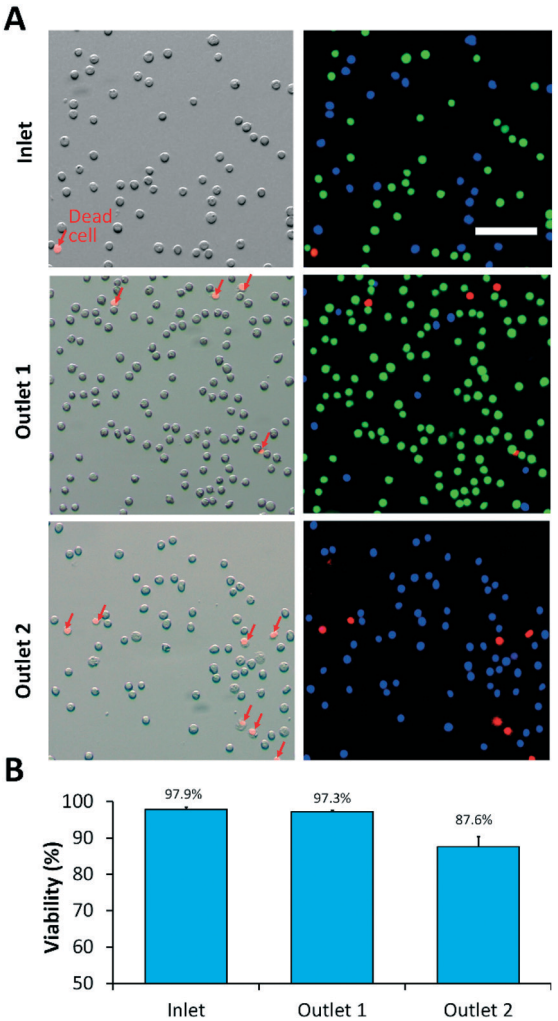

Fig. 7 Cell viability results. (A) Composite images showing the ratio of dead cells collected at the inlet and outlets. PI staining was used to test the cell viability. The dead cells showed red fluorescence. (B) Quantitative characterization of cell viability collected at the inlet and outlets. Each error bar represents the standard deviation of three independent experiments. Scale bar = 100 μm.

path of the cells in the DEP separation region. Increasing DEP force means inducing larger electric field, which may degrade the viability of the cells. Thus, the way of extending the flow path in the DEP region is more preferable. For instance, the serpentine channel can be used to extend the flow path in the DEP region (Fig. S7†).

Fig. 7 illustrates the viability of the separated cells. PI staining was used to mark the dead cells with red fluorescence. The viability of the cells before flowing through the DEP separator was 97.9%. After flowing through the separator with a 5 MHz and 12 V_{p-p} sinusoidal voltage applied, the viability of the cells collected at outlets 1 and 2 were 97.3% and 87.6%, respectively. The cells that experienced a lower DEP force and flowed into outlet 1 had almost the same viability as the cells at the inlet, whereas the viability of the cells deflected by the strong DEP force to outlet 2 was reduced by approximately 10%. The probable reason is that the large DEP force had a chance to break the cell membrane and thus degraded the cell viability. Despite that the electric field degraded the cell viability, the use of DEP technology can potentially benefit a higher yield and purity in separating those previously unknown cell subpopulations in comparison to the existing micro-filtration and inertial methods based on cell size difference only. Gravitational sedimentation combined with DEP technology considers the differences in both the size and dielectric property of cells.

Conclusions

This paper reports the development of a sheathless approach for the separation of cells with different sizes or dielectric properties. The proposed method utilised integrated gravitational-sedimentation-based sheathless prefocusing and DEP separation technologies in a simple microfluidic separator for the continuous and label-free separation of cells. Sheathless cell focusing was realized by using the gravitational sedimentation of cells in a tubing inserted into the inlet of the microfluidic chip with an adjustable steer angle. Through the use of an interdigitated electrode array located at the bottom of the microchannel, a DEP force that deflects the motion of the targeted cells and separate the cell mixture can be generated. The effectiveness of the proposed approach was demonstrated by separating THP-1 cells from yeast cells on the basis of size, and the THP-1 cells were separated from the OCI-AML3 cells on the basis dielectric property. The experimental results indicated that the proposed simple and flexible approach can efficiently separate cells not only by size but also by dielectric property. Moreover, this approach facilitates the easy integration of DEP separation with other microfluidic functionalities to achieve system miniaturisation for potential applications in clinical and biological fields.

Conflicts of interest

There are no conflicts to declare.

Acknowledgements

This work was supported by the Research Grants Council of the Hong Kong Special Administrative Region, China (Reference No. N_CityU102/15, and CityU11209917).

References

1 B. D. Plouffe, S. K. Murthy and L. H. Lewis, *Rep. Prog. Phys.*, 2015, **78**, 16601.
2 D. R. Gossett, W. M. Weaver, A. J. Mach, S. C. Hur, H. Tse Tat Kwong, W. Lee, H. Amini and D. Di Carlo, *Anal. Bioanal. Chem.*, 2010, **397**, 3249–3267.
3 J. D. Adams, U. Kim and H. T. Soh, *Proc. Natl. Acad. Sci. U. S. A.*, 2008, **105**, 18165–18170.
4 S. A. Khashan, E. P. Furlani, H. Seo and Y. Kim, *J. Phys. D: Appl. Phys.*, 2007, **40**, 1313.
5 K. E. Mccloskey, J. J. Chalmers and M. Zborowski, *Anal. Chem.*, 2003, **75**, 6868–6874.

6 N. Pamme and C. Wilhelm, *Lab Chip*, 2006, **6**, 974–980.
7 A. Ashkin, J. M. Dziedzic and T. Yamane, *Nature*, 1987, **330**, 769–771.
8 X. Wang, S. Chen, M. Kong, Z. Wang, K. D. Costa, R. A. Li and D. Sun, *Lab Chip*, 2011, **11**, 3656–3662.
9 Y. Huang, S. Joo, M. Duhon, M. Heller, B. Wallace and X. Xu, *Anal. Chem.*, 2002, **74**, 3362–3371.
10 X. Wang, J. Yang, Y. Huang, J. Vykoukal, F. F. Becker and P. R. C. Gascoyne, *Anal. Chem.*, 2000, **72**, 832–839.
11 J. Park, B. Kim, K. Choi, S. Hong, H. Lee and K. Lee, *Lab Chip*, 2005, **5**, 1264–1270.
12 F. Petersson, A. Lena, A. Swa and T. Laurell, *Anal. Chem.*, 2007, **79**, 5117–5123.
13 P. Augustsson, C. Magnusson, M. Nordin, H. Lilja and T. Laurell, *Anal. Chem.*, 2012, **84**, 7954–7962.
14 S. Choi, T. Ku, S. Song and J. Park, *Lab Chip*, 2011, **11**, 413–418.
15 S. Choi, S. Song, C. Choi and J. Park, *Lab Chip*, 2007, **7**, 1532–1538.
16 Y. Cheng, X. Ye, Z. Ma, S. Xie and W. Wang, *Lab Chip*, 2016, **16**, 1–11.
17 Y. Cheng, Y. Wang, Z. Ma, W. Wang and X. Ye, *Lab Chip*, 2016, **16**, 4517–4526.
18 X. Li, W. Chen, G. Liu, W. Lu and J. Fu, *Lab Chip*, 2014, **14**, 2565–2575.
19 M. Pødenphant, N. Ashley, K. Koprowska, K. U. Mir, M. Zalkovskij, B. Bilenberg, W. Bodmer, A. Kristensen and R. Marie, *Lab Chip*, 2015, **15**, 4598–4606.
20 D. Di Carlo, *Lab Chip*, 2009, **9**, 3038–3046.
21 E. Sollier, D. E. Go, J. Che, D. R. Gossett, S. O. Byrne, W. M. Weaver, N. Kummer, M. Rettig, J. Goldman, N. Nickols, S. Mccloskey, P. Kulkarni and D. Di, *Lab Chip*, 2014, **14**, 63–77.
22 S. C. Hur, N. K. Henderson-Maclennan, E. Mccabe and D. Di Carlo, *Lab Chip*, 2011, **11**, 912–920.
23 J. Sun, M. Li, C. Liu, Y. Zhang, D. Liu, W. Liu, G. Hu and X. Jiang, *Lab Chip*, 2012, **12**, 3952–3960.
24 W. Liu and J. Wang, *Lab Chip*, 2017, **17**, 3578–3591.
25 D. Huh, J. H. Bahng, Y. Ling, H. Wei, O. D. Kripfgans, J. B. Fowlkes, J. B. Grotberg and S. Takayama, *Anal. Chem.*, 2007, **79**, 1369–1376.
26 E. Ozkumur, A. M. Shah, J. C. Ciciliano, B. L. Emmink, T. David, E. Brachtel, M. Yu, P. Chen, B. Morgan, J. Trautwein, A. Kimura, S. Sengupta, S. L. Stott, N. M. Karabacak, T. A. Barber, J. R. Walsh, K. Smith, P. S. Spuhler, J. P. Sullivan, R. J. Lee, D. T. Ting, X. Luo, A. T. Shaw, A. Bardia, V. Lecia, D. N. Louis, S. Maheswaran, R. Kapur and D. A. Haber, *Sci. Transl. Med.*, 2013, **5**, 1–20.
27 M. M. Wang, E. Tu, D. E. Raymond, J. M. Yang, H. Zhang, N. Hagen, B. Dees, E. M. Mercer, A. H. Forster, I. Kariv, P. J. Marchand and W. F. Butler, *Nat. Biotechnol.*, 2005, **23**, 83–87.
28 S. I. Cheng and W. Su, *Lab Chip*, 2015, **15**, 2950–2959.
29 V. Gupta, I. Jafferji, M. Garza, V. O. Melnikova, D. K. Hasegawa, R. Pethig and D. W. Davis, *Biomicrofluidics*, 2012, **6**, 1–14.
30 K. Han and A. B. Frazier, *Lab Chip*, 2008, **8**, 1079–1086.
31 S.-I. Han, S.-M. Lee, Y.-D. Jooc and K.-H. Han, *Lab Chip*, 2011, **11**, 3864–3872.
32 P. Renaud, *Biomicrofluidics*, 2011, **5**, 34122.
33 D. Chen, J. A. Thomson, C. D. Meinhart and H. T. Soh, *Electrophoresis*, 2008, **29**, 1213–1218.
34 B. Prabhakarpandian, K. Pant, G. J. Klarmann and A. Perantoni, *Lab Chip*, 2015, **15**, 1320–1328.
35 M. Kanai, S. Ikeda, J. Tanaka and J. Sang, *Sens. Actuators, A*, 2004, **111**, 32–36.
36 C.-P. Jen, C.-H. Weng and C.-T. Huang, *Electrophoresis*, 2011, **32**, 2428–2435.
37 Y. Ren, J. Liu, W. Liu, Q. Lang, Y. Tao, Q. Hu, L. Hou and H. Jiang, *Lab Chip*, 2016, **16**, 2803–2812.
38 M. F. M. Speetjens and A. A. Van Steenhoven, *Microfluid. Nanofluid.*, 2015, **18**, 1115–1129.
39 X. Chen, Y. Ren, W. Liu, X. Feng, Y. Jia, Y. Tao and H. Jiang, *Anal. Chem.*, 2017, **89**, 9583–9592.
40 J. Zhang, S. Yan, D. Yuan, G. Alici, N.-T. Nguyen, M. E. Warkiani and W. Li, *Lab Chip*, 2016, **16**, 10–34.
41 S. C. Hur, T. K. H. Tseb and D. Di Carlo, *Lab Chip*, 2010, **10**, 274–280.
42 A. J. Chung, D. Pulido, J. C. Oka, H. Amini, M. Masaeli and D. Di Carlo, *Lab Chip*, 2013, **13**, 2942–2949.
43 P. Paiè, F. Bragheri, D. Di Carlo and R. Osellame, *Microsyst. Nanoeng.*, 2017, **3**, 1–8.
44 S. Song and S. Choi, *J. Chromatogr. A*, 2013, **1302**, 191–196.
45 K. J. Morton, K. Loutherback, D. W. Inglis, O. K. Tsui, J. C. Sturm, S. Y. Chou and R. H. Austin, *Proc. Natl. Acad. Sci. U. S. A.*, 2008, **105**, 7434–7438.
46 K. Loutherback, J. D. Silva, L. Liu, A. Wu, R. H. Austin and J. C. Sturm, *AIP Adv.*, 2012, **2**, 42107.
47 D. Yuan, Q. Zhao, S. Yan and D. Yuan, *Lab Chip*, 2018, **18**, 551–567.
48 G. Romeo, G. D. Avino, F. Greco, P. A. Netti and P. L. Maffettone, *Lab Chip*, 2013, **13**, 2802–2807.
49 S. Yang, J. Y. Kim, S. J. Lee, S. S. Lee and J. M. Kim, *Lab Chip*, 2011, **11**, 266–273.
50 S. H. Yang, D. J. Lee, J. R. Youn and Y. S. Song, *Anal. Chem.*, 2017, **89**, 3639–3647.
51 S. Yan, J. Zhang, Y. Yuan, G. Lovrecz, G. Alici, H. Du, Y. Zhu and W. Li, *Electrophoresis*, 2015, **36**, 284–291.
52 S. Yan, J. Zhang, G. Alici, H. Du, Y. Zhu and W. Li, *Lab Chip*, 2014, **14**, 2993–3003.
53 S. Yan, J. Zhang, D. Yuan and W. Li, *Electrophoresis*, 2017, **38**, 238–249.
54 J. P. Beech, J. Peter and J. O. T. Tegenfeldt, *Lab Chip*, 2009, **9**, 2698–2706.
55 N. M. Karabacak, P. S. Spuhler, F. Fachin, E. J. Lim, E. Ozkumur, J. M. Martel, N. Kojic, K. Smith, P. Chen, H. Hwang, B. Morgan, J. Trautwein, T. A. Barber and L. Shannon, *Nat. Protoc.*, 2014, **9**, 694–710.
56 B. Alvin, S. Seshadri and J. Brown, *Blood*, 1976, **48**, 361–371.
57 A. K. Bryan, A. Goranov, A. Amon and S. R. Manalis, *Proc. Natl. Acad. Sci. U. S. A.*, 2010, **107**, 999–1004.

58 W. H. Grovera, A. K. Bryana, M. Diez-Silvac, S. Sureshb, E. J. M. Higginsf and S. R. Manalisa, *Proc. Natl. Acad. Sci. U. S. A.*, 2011, **108**, 10992–10996.
59 R. Polanowska-grabowska and R. L. Gear, *Br. J. Haematol.*, 1992, **82**, 715–720.
60 P. M. Hinderliter, K. R. Minard, G. Orr, W. B. Chrisler, B. D. Thrall, J. G. Pounds and J. G. Teeguarden, *Part. Fibre Toxicol.*, 2010, **7**, 1–20.
61 Y. Wei, Z. Xu, M. A. Cachia, J. Nguyen and Y. Zheng, *J. Micromech. Microeng.*, 2016, **26**, 95006.
62 E. A. Henslee, E. Schmelz and V. T. Forest, *Electrophoresis*, 2011, **32**, 3164–3171.
63 S. Patel, D. Showers, P. Vedantam, T. Tzeng and S. Qian, *Biomicrofluidics*, 2012, **6**, 34102.
64 G. H. Markx and C. L. Davey, *Enzyme Microb. Technol.*, 1999, **25**, 161–171.